Inorganic Chemistry

Article

pubs.acs.org/IC

To Bend or Not To Bend: Experimental and Computational Studies of Structural Preference in Ln(Tp^{iPr}_2)$_2$ (Ln = Sm, Tm)

Aurélien Momin,[§,∥] Lee Carter,[†,#] Yi Yang,[†] Robert McDonald,[†] Stéphanie Essafi (née Labouille),[§,△] François Nief,[§] Iker Del Rosal,[‡] Andrea Sella,*[,⊥] Laurent Maron,*[,‡] and Josef Takats*[,†]

[†]Department of Chemistry, University of Alberta, Edmonton, AB, Canada T6G 2G2

[‡]Laboratoire de Physique et Chimie des Nanoobjets, INSA, Université Paul Sabatier, 135 Avenue de Rangueil, 31077 Toulouse Cedex, France

[§]Laboratoire de Chimie Moléculaires, CNRS, Ecole Polytechnique, 91128 Palaiseau, France

[⊥]Department of Chemistry, University College London, 20 Gordon Street, London, WC1H 0AJ, United Kingdom

Supporting Information

ABSTRACT: The synthesis and characterization of Ln(Tp^{iPr2})$_2$ (Ln = Sm, **3Sm**; Tm, **3Tm**) are reported. While the simple ^{1}H NMR spectra of the compounds indicate a symmetrical solution structure, with equivalent pyrazolyl groups, the solid-state structure revealed an unexpected, "bent sandwich-like" geometry. By contrast, the structure of the less sterically congested Tm($Tp^{Me2,4Et}$)$_2$ (**4**) adopts the expected symmetrical structure with a linear B−Tm−B arrangement. Computational studies to investigate the origin of the unexpected bent structure of the former compounds indicate that steric repulsion between the isopropyl groups forces the Tp ligands apart and permits the development of unusual interligand C−H···N hydrogen-bonding interactions that help stabilize the structure. These results find support in the similar geometry of the Tm(III) analogue [Tm(Tp^{iPr2})$_2$]I, **3Tm**$^+$, and confirm that the low symmetry is not the result of a metal−ligand interaction. The relevance of these results to the general question of the coordination geometry of MX_2 and M(C_5R_5)$_2$ (M = heavy alkaline earth and Ln(II), X = halide, and C_5R_5 = bulky persubstituted cyclopentadienyl) complexes and the importance of secondary H-bonding and nonbonding interactions on the structure are highlighted.

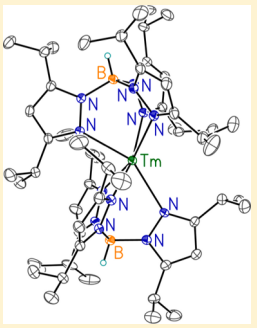

INTRODUCTION

The structure and bonding of the s-block and the lanthanides are usually described as predominantly ionic. The absence, in most cases, of specific directional interactions means that it is typical to expect high-symmetry structures.[1] Deviations from these symmetries have often given rise to vigorous discussion. For example, the discovery that, in the gas phase, the heavy alkaline earth halides adopted a bent geometry at the metal[2,3] led to a long debate over the relative contributions of polarization and d-orbital participation.[4]

Among the lanthanides, the classic example of this was provided by Evans with his report of the iconic molecule [Sm(η-C_5Me_5)$_2$(THF)$_2$][5] and its unsolvated analogue, [Sm(η-C_5Me_5)$_2$],[5−7] which have very similar bent metallocene structures. The isolation of the Eu and Yb analogues,[8] followed by those of Ca, Sr, and Ba,[9,10] engendered several computational studies[11−15] to try to understand the nature of the distortion from the C_5-symmetric linear sandwich structure. These studies have led to the view that the distortion arises predominantly from the attractive dispersion/van der Waals interactions.[11,16]

Although these distortions are observed consistently, the energy barrier separating the bent and linear sandwich geometries is rather small since the geometrical preference can be easily manipulated by changing the steric profile of the cyclopentadienyl ligands. Thus, bis-cyclopentadienyl Ln(II) and related alkaline earth metal compounds with the very bulky $C_5{}^iPr_5$,[17,18] C_5Ph_5,[19] and Cp^{BIG} (Cp^{BIG} = C_5(4-n-Bu-C_6H_4)$_5$)[20−22] all adopt parallel-ring sandwich arrangements. Harder attributes the S_{10} symmetry in the latter compounds to favorable, nonclassical C−H···π(phenyl) ring interactions. Another noteworthy feature of these complexes is the observation that the metal sits away from the center of the molecule, allowing for dynamics; these alkaline earth and lanthanide structures have been discussed and rationalized in terms of a polarization model.[22,23]

Such structural diversity is even more pronounced for complexes based on Trofimenko's hydrotris(pyrazolyl)-borates,[24,25] which are also significantly influenced by the substitution pattern of the ligand set. (The abbreviation we will use for these ligands is that proposed by Trofimenko: Tp stands for tris(pyrazolyl)borate; R and R′ are substituents at the 3- and 5-positions of the pyrazolyl group, respectively, and the 4-substituent is denoted by the superscript 4R.)

Some time ago two of us reported the synthesis, spectroscopic properties, and solid-state structures of Ln(Tp^{Me2})$_2$ (Ln = Sm, **1Sm**; Yb, **1Yb**) and some related complexes.[26−29] We anticipated that the greater cone angle of Tp^{Me2} (239°)[24] compared to the C_5Me_5 ligand (142°)[30] would

Received: July 31, 2014
Published: October 27, 2014

   dx.doi.org/10.1021/ic501816v | *Inorg. Chem.* 2014, 53, 12066−12075

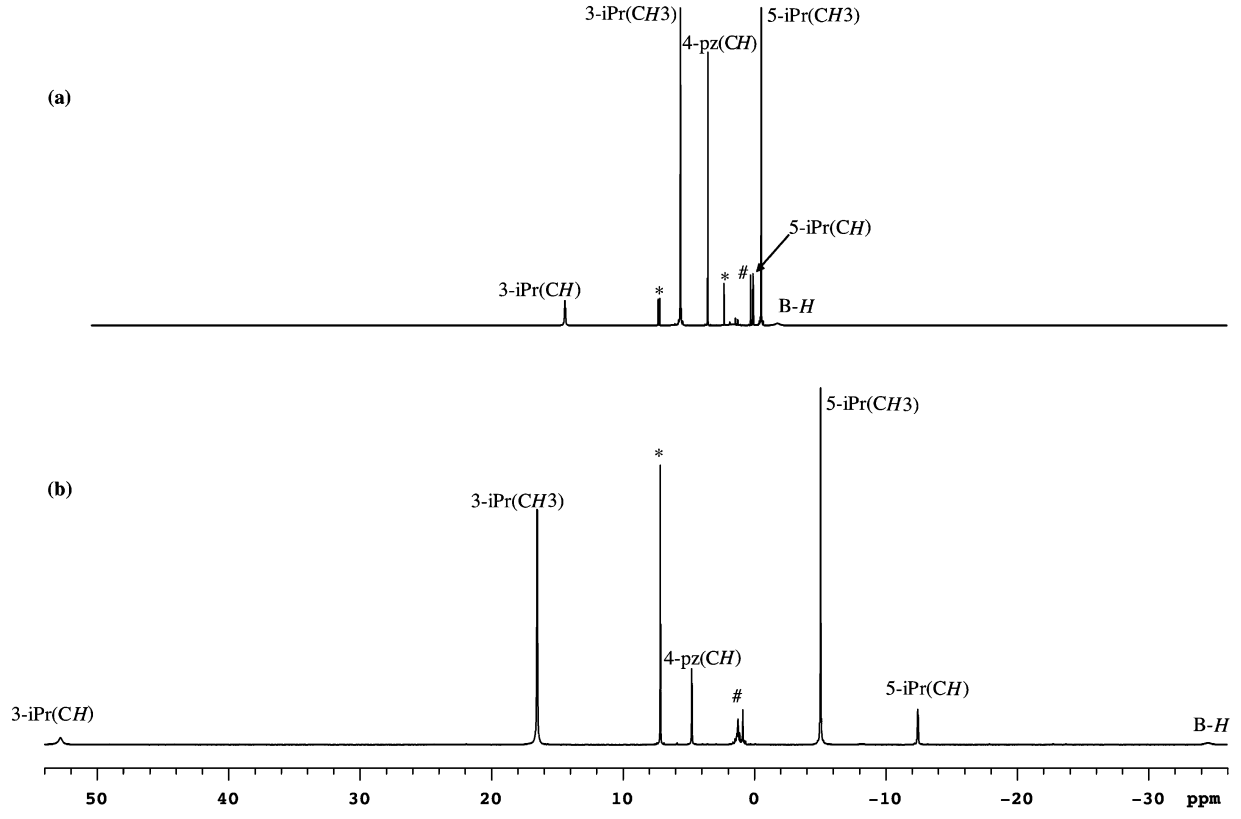

Figure 1. RT ^{1}H NMR spectra of Ln(Tp^{iPr2})$_2$. (a) Ln = Sm (**3Sm**) in toluene-d_8, $^{\#}$silicone grease; (b) Ln = Tm (**3Tm**) in benzene-d_6, $^{\#}$pentane. In both spectra, * is residual solvent peaks.

confer significantly greater steric control over the metal center. This proved to be the case, and the more congested Ln(Tp^{Me2})$_2$ complexes were isolated as THF-free materials; the solid-sate structure proved to be highly symmetrical, adopting a trigonal antiprismatic coordination geometry with colinear B−Ln−B atoms and S_6 molecular symmetry, a "sandwich-like" structure. This high symmetry was, however, accompanied by an unexpected lack of solubility, although solubility could be increased substantially by introducing an ethyl substituent in the 4-position of the pyrazolyl groups.

This coordination environment was found to give a good balance of kinetic stabilization and reactivity, allowing the isolation of a variety of seven-coordinate complexes, Sm(Tp^{Me2})$_2$X,[28] and even eight-coordinate, Sm(Tp^{Me2})$_2$XY, complexes[26,31] from reaction with reducible substrates.

Pushing the steric congestion even further, increasing the bulk in the 3-position of the pyrazolyl rings and using the superbulky Tp^{tBu,Me} ligand led to a change in structure. In the homoleptic Ln(Tp^{tBu,Me})$_2$ (Ln = Sm, Yb)[32] molecules, one scorpionate switched from the classical κ^3-N$_3$ bonding mode to being coordinated by two nitrogens and one "agostic" B−H bond, i.e., a κ^3-N$_2$H Tp^{tBu,Me} ligand.[32] This interesting structural motif is maintained in solution, as shown by VT ^{1}H NMR studies, which also revealed fascinating two-stage dynamic behavior: a low-energy process involving the κ^3-N$_2$H ligand, and high-energy process which results in exchange of the coordination mode of the two distinct scorpionates.

Questions therefore arise regarding the structural preferences of Ln(Tp$^{R,R'}$)$_2$ complexes for ligands with a steric demand and cone angle intermediate between those of Tp^{Me2} and Tp^{tBu,Me}. The Tp^{iPr2} ligand appeared to fit the bill, since, with the typical conformational preference for the ^{i}Pr substituents to place the C−H bond pointing toward the B and metal centers,[33,34] it presents an interior to the metal center analogous to that of the Tp^{Me2} ligand, while its exterior resembles that of Tp^{tBu,Me}, and with steric demand expected to fall somewhere between the two. [Although cone angles are sometimes used in the discussion of the steric demand of scorpionate ligands, care must be exercised. The most consistent values seem to be based on the structures of a series of monomeric Tl(I) scorpionate complexes,[24,25] but even these values should be used with caution. Thus, the relevant values for the present purpose are Tp^{Me2} 239°, Tp^{iPr,4Br} 243°, and Tp^{tBu,Me} 243°, implying similar size for Tp^{iPr2} and Tp^{tBu,Me} ligands. However, in TlTp^{iPr,4Br} the ^{i}Pr methyl substituents point toward Tl and not away, as it is more commonly observed. Hence, not surprisingly, the cone angle is the same as in the Tp^{tBu,Me} ligand. There are independent geometrical features and reactivity behavior that indicate that the steric profile of the ^{i}Pr-substituted Tp ligand is smaller than that of the corresponding ^{t}Bu-substituted ligand,[35] and we support this conclusion. What is clear is that the low barriers to alkyl group rotation in Tp-type ligands make it appropriate that estimates of their cone angles should be accompanied by much larger error bars than the rather simplistic figures typically quoted suggest.]

In this article we report the synthesis and solid-state structure of Ln(Tp^{iPr2})$_2$ (Ln = Sm, **3Sm**; Tm, **3Tm**), highly sterically congested complexes that have been found to adopt an unexpected "bent-sandwich-like" geometry. We have used DFT to probe the intramolecular origins of this origins of this unusual distortion. The solid-state structures of the oxidized analogue of **3Tm**, [Tm(Tp^{iPr2})$_2$]I (**3Tm**$^{+}$), and Tm(Tp^{Me2,4Et})$_2$ (**4**) are also reported.

dx.doi.org/10.1021/ic501816v | Inorg. Chem. 2014, 53, 12066−12075

RESULTS AND DISCUSSION

Synthesis and Characterization of Ln(Tp^{iPr2})$_2$ (Ln = Sm, Tm). Addition of two equivalents of KTp^{iPr2}, dissolved in THF, to a solution of LnI_2 in the same solvent resulted in an immediate color change from blue (Sm) or green (Tm) to green and reddish-brown, respectively, and the precipitation of KI, eq 1. After workup the Ln(Tp^{iPr2})$_2$ (Ln = Sm, **3Sm**; Tm, **3Tm**) compounds were obtained as green (Sm) and plum-red (Tm) fluffy solids, sufficiently pure for further reactions.

$$LnI_2 + 2KTp^{iPr2} \rightarrow Ln(Tp^{iPr2})_2 + 2KI(\downarrow) \quad (1)$$

The Sm compound is moderately stable at room temperature and can be kept at −35 °C for months but then shows signs of decomposition. The Tm compound, however, is significantly less thermally stable and starts to decompose even at −35 °C after a week, giving insoluble white powders of unknown composition.

The compounds are extremely soluble in ether and hydrocarbon solvents, and crystallization from these solvents proved challenging (see Experimental Section), but eventually led to crystals suitable for X-ray analysis and NMR studies.

The ^{1}H NMR spectra of **3Sm** and **3Tm** are shown in Figure 1. The spectra establish the purity of these delicate and highly air sensitive compounds. The spectra exhibit one set of pyrazolyl group resonances with the expected intensity ratio. The signals are paramagnetically shifted, and the two spectra provide a nice illustration of the greater shifts induced by thulium with its greater magnetic moment.[36,37] The simple spectra show no broadening of the resonances down to −80 °C, implying either a symmetrical structure, similar to the previously reported Ln(Tp$^{R,R'}$)$_2$,[26−28] or a time-averaged structure due to rapid fluxionality. To resolve the ambiguity, the solid-state structures of **3Sm** and **3Tm** were determined by single-crystal X-ray diffraction.

Solid-State Structure of Ln(Tp^{iPr2})$_2$ (Ln = 3Sm, 3Tm). The structures of **3Sm** and **3Tm**, with their respective numbering schemes, are shown in Figure 2; relevant metrical parameters are listed in Table 1.

Close examination of Figure 2 reveals that the molecular geometry of both of these complexes is different both from the linear sandwich-like structures of Ln(Tp^{Me2})$_2$[26−28] and from that of the highly congested Ln(Tp^{tBu,Me})$_2$ that feature a κ^3-N$_2$H-Tp^{tBu,Me} ligand.[32] The Tp^{iPr2} ligands in complexes **3** display the classical κ^3-bonding mode, but the B1−Ln−B2 angle is not 180°. Instead it is significantly reduced to 150.1° (**3Sm**) and 152.2° (**3Tm**), a structural motif that has not been observed before in the absence of either an additional ligand (e.g., Sm(Tp^{Me2})$_2$X)[28] or a stereochemically active lone pair in the coordination sphere (as in M(Tp^{Me2})$_2$, M = Sn, Pb).[38,39] The distortion of the metal's coordination sphere is also reflected in the ca. 30° angle between the Tp^{iPr2} ligand's coordination plane (i.e., the angle between planes N12N22N32/N42N52N62). The "bent" geometry is reminiscent of the bent-sandwich structure of [Sm(C$_5$Me$_5$)$_2$].[6] Indeed the molecular symmetry is "close" to C_s, the mirror plane running through B1LnB2, with N51N52 deviating only slightly, but N21N22 more so, from this plane (see Table SI 1).

The bending of the Tp^{iPr2} ligands along the BNB line and the molecular symmetry of complexes **3** are also distinct from that of seven-coordinate Sm(Tp^{Me2})$_2$X (X = F, Cl).[28] In the latter, the cavity accommodating the X ligand is achieved not just by simple bending of the BSmB angle but also by twisting and

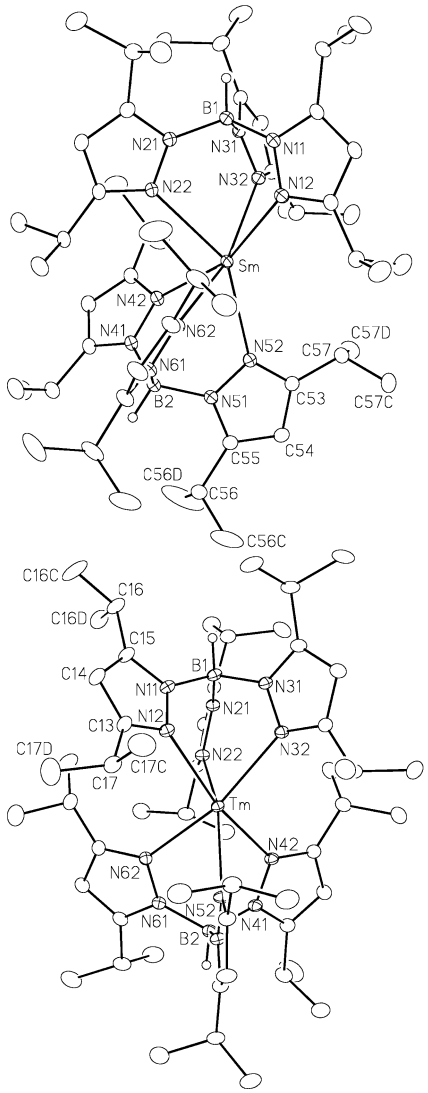

Figure 2. Molecular structures of (a, above) **3Sm**, viewed perpendicular to the B1SmB2 plane (side view), and (b, below) **3Tm**, viewed perpendicular to the N12N32N53 plane (front view); showing the "bent sandwich" geometry (above) and the close to C_s symmetry (below). The atoms are drawn with 20% probability ellipsoids. Hydrogen atoms have been omitted for clarity.

bending of the two Tp^{Me2} ligands around the B−N bond, resulting in an approximate C_2-symmetric structure in the solid state. Nevertheless, symmetrization of both C_s and C_2 structures is a very low activation process, as seen by the simple and temperature-invariant ^{1}H NMR spectra of these complexes.

The "bent-sandwich" geometry of complexes **3** has as its result an expansion of the N12N32N52 and contraction of the N22N42N62 triangular faces ("front" and "back" in Figure 2b), as seen by the much larger N−Ln−N(inter ligand)$_{cis}$ angles: N12−Ln−N52/N32−Ln−N52, 122.5°$_{av}$ compared to N22−Ln−N42/N22−Ln−N62, 86.0°$_{av}$. Viewing it this way, the coordination geometry could be described as "capped octahedral" with the capping position on the N12N32N52 face missing. Indeed, in spite of the bending along the B1LnB2 line, the two triangular faces, N12N32N52/N22N42N62, are close to being parallel (angles: **3Sm** 12°, **3Tm** 13°).

The opposite change in the degree of congestion of these two faces is also reflected in the LnNNB torsional and

dx.doi.org/10.1021/ic501816v | Inorg. Chem. 2014, 53, 12066−12075

Table 1. Interatomic Distances (Å) and Angles (deg) for $Sm(Tp^{iPr2})_2$ (3Sm), $Tm(Tp^{iPr2})_2$ (3Tm), and $[Tm(Tp^{iPr2})_2]I$ ($3Tm^+$)

	3Sm(A)[a]	3Sm(B)[a]	3Tm(A)[a]	3Tm(B)[a]	$3Tm^+$
Ln−N12	2.638(2)	2.664(2)	2.534(2)	2.538(2)	2.426(2)
Ln−N22	2.668(2)	2.639(2)	2.543(2)	2.536(2)	2.413(2)
Ln−N32	2.645(2)	2.664(2)	2.553(2)	2.534(2)	2.379(2)
Ln−N42	2.587(2)	2.624(2)	2.500(2)	2.518(2)	2.376(2)
Ln−N52	2.680(2)	2.643(2)	2.599(2)	2.554(2)	2.438(2)
Ln−N62	2.605(2)	2.616(2)	2.488(2)	2.503(2)	2.378(2)
$Ln-N_{range}$	2.59−2.68	2.62−2.66	2.49−2.60	2.50−2.55	2.38−2.44
N−Ln−N(intra)					
N12−Ln−N22	78.68(5)	77.34(5)	81.80(7)	80.59(7)	88.27(6)
N12−Ln−N32	69.08(5)	70.85(5)	71.42(7)	71.41(7)	74.32(6)
N22−Ln−N32	77.52(5)	78.85	81.87(7)	83.53(7)	82.93(6)
N42−Ln−N52	69.71(5)	73.80(5)	76.12(7)	76.45(7)	76.16(5)
N42−Ln−N62	81.45(5)	83.05(5)	86.03(5)	87.69(7)	88.26(5)
N52−Ln−N62	72.96(5)	68.86(5)	72.61(7)	72.54(7)	80.84(5)
$N-Ln-N(inter)_{cis}$					
N12−Ln−N52	127.86(5)	122.71(6)	119.32(7)	118.87(7)	111.87(6)
N12−Ln−N62	101.05(5)	102.59(5)	99.84(7)	100.62(7)	97.22(6)
N22−Ln−N42	84.17(5)	87.48(5)	84.94(7)	86.31(7)	85.61(5)
N22−Ln−N62	84.93(5)	87.93(5)	84.33(7)	87.59(7)	78.70(5)
N32−Ln−N42	104.24(5)	100.09(5)	99.42(7)	98.32(7)	98.14(6)
N32−Ln−N52	125.83(5)	124.92(6)	122.61(7	117.86(8)	119.03(6)
$N-Ln-N(inter)_{trans}$					
N12−Ln−N42	162.34(5)	163.49(5)	164.4(7)	164.10(7)	170.84(6)
N22−Ln−N52	147.69(5)	151.43(5)	150.88(7)	153.94(7)	152.90(5)
N32−Ln−N62	161.18(6)	166.20(6)	164.60(7)	168.91(8)	160.03(6)
$N-Ln-N_{(inter)trans}$					
N12−Ln−N42	162.34(5)	163.49(5)	164.4(7)	164.10(7)	170.84(6)
N22−Ln−N52	147.69(5)	151.43(5)	150.88(7)	153.94(7)	152.90(5)
N32−Ln−N62	161.18(6)	166.20(6)	164.60(7)	168.91(8)	160.03(6)
Torsion Angles					
Ln−N12N11−B1	8.5(2)	33.3(2)	32.5(3)	30.9(3)	0.8(2)
Ln−N22−N21−B1	23.5(2)	28.7(2)	22.3(3)	24.1(3)	26.4(2)
Ln−N32−N31−B1	32.8(2)	17.2(2)	6.6(3)	3.9(3)	26.8(2)
Ln−N42−N41−B2	22.8(2)	7.4(2)	9.1(3)	11.6(3)	22.6(2)
Ln−N52−N51−B2	1.3(2)	2.5(2)	2.3(3)	0.6(3)	3.3(2)
Ln−N62−N61−B2	7.1(2)	30.7(2)	22.8(3)	28.2(3)	3.2(2)
B1−Ln−B	148.34(5)	151.79(5)	151.13(7)	153.40(7)	152.59(5)

[a]There are two independent molecules per asymmetric unit.

intraligand angles. Thus, in the expanded N12N32N52 face, the LnN52N51B2 torsional angles are close to zero and result in easy nestling of the N51N52 pyrazolyl ring and its 3-^{i}Pr substituent between the N12/N32 pyrazolyl groups; these retain the typical, small intraligand N12−Ln−N32 angle of ca. 70°. On the other hand, in the contracted N22N42N62 face, the Ln−N22−N21−B1 torsional angles are greater than 20° and the intraligand N42−Ln−N62 angles have opened up to over 80° to accommodate the 3-^{i}Pr substituent of the N21N22 pyrazolyl ring. As expected, the N42−Tm−N62 angle ($86.4°_{av}$) has opened up more than in **3Sm** because of the smaller and more congested Tm(II) center.

It is noteworthy that, in spite of the distortion, the Sm−N distances in **3Sm** remain similar to those observed in the related $Sm(Tp^{R,R'})_2$ complexes.[26−28] For **3Tm**, the decrease of 0.1 Å in the Ln−N distance compared with **3Sm** is in line with the reduction in the six-coordinate ionic radius from Sm(II) to Tm(II).[40] However, the Tm−N distances are shorter than in the four-coordinate $Tm(Tp^{tBu,Me})N(SiMe_3)_2/CH(SiMe_3)_2$ complexes,[41] an indication of the ability of the $Tp^{R,R'}$ ligands to interlock efficiently.

As often found in complexes with Tp^{iPr2} ligands,[33,34] most of the ^{i}Pr substituents are arranged such that the C−H bonds point toward either the B−H bond or the Ln center, to minimize steric crowding. However, some of the ^{i}Pr substituents around the contracted triangular face exhibit subtly different conformational orientation, and possible reasons for this will be discussed in the Computational Studies subsection.

These structural studies revealed that both complexes **3Sm** and **3Tm** crystallize with *two* independent molecules per asymmetric unit. Although the distances and angles in Table 1 show some small variations, by and large the two independent molecules are very similar, clearly indicating that the observed "bent-sandwich" geometry is not the result of packing forces in the crystal, but it is an inherent feature of complexes **3**.

Synthesis and Solid-State Structure of $Tm(Tp^{Me2,4Et})_2$ (4Tm). To complete the picture and to rule out the possibility that the "bent" geometry was an inherent feature of $Tm(Tp^{R,R'})$ complexes, a less crowded complex was contemplated. In view of the thermal sensitivity of $Tm(Tp^{iPr2})_2$ and the anticipated

dx.doi.org/10.1021/ic501816v | Inorg. Chem. 2014, 53, 12066−12075

insolubility of $Tm(Tp^{Me2})_2$, attention was focused on the soluble compound $Tm(Tp^{Me2,4-Et})_2$.

The reaction of TmI_2 with $KTp^{Me2,4Et}$ was carried out in DME, a solvent in which Tm(II) compounds are known to be more stable.[42] This approach gave good-quality $Tm(Tp^{Me2,4Et})_2$ (**4Tm**), after crystallization. However, even pure samples of **4Tm** in DME or THF at RT start to deposit white solids of unknown composition after a few hours, and the same happens when solid **4Tm**, stored at −35 °C for a few days, is redissolved in the same solvents. Nevertheless, the compound is stable enough to give a ^1H NMR spectrum in C_6D_6 at RT. The spectrum shows a simple pattern, one signal each for the 3- and 5-Me groups and CH_2 and CH_3 of the 4-Et substituent, consistent with a symmetrical sandwich-like or a time-averaged symmetrical solution structure. The solid-state X-ray structure confirms the former.

Compound **4Tm** is isomorphous to the Tm analogue $Sm(Tp^{Me2,4Et})_2$,[28] with the Sm atom on a center of inversion, Figure 3. The metrical parameters, Table 2, are very similar to

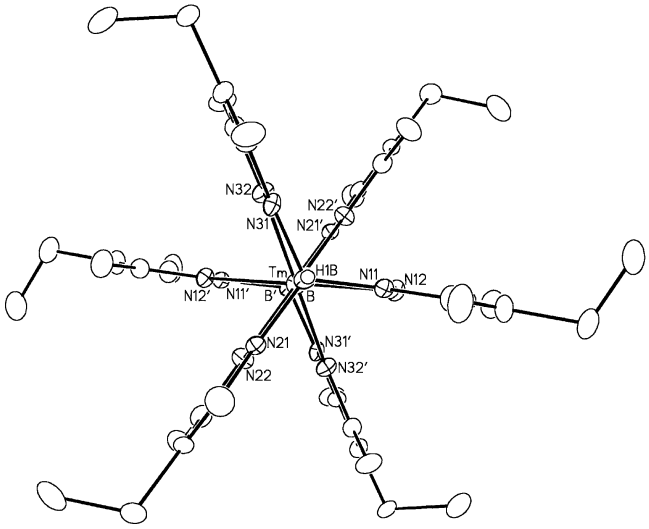

Figure 3. Molecular structure of **4Tm** viewed down the B---Tm---B axis, showing the disposition of the ethyl groups. The atoms are drawn with 20% probability ellipsoids. Hydrogen atoms have been omitted for clarity. Primed atoms are related to unprimed ones via the crystallographic inversion center (0, 0, 0) on which the Tm atom is located.

Table 2. Interatomic Distances (Å) and Angles (deg) for $Tm(Tp^{Me2,4Et})_2$ (4Tm)

Tm−N12		2.482(5)	
Tm−N22		2.473(6)	
Tm−N32		2.476(6)	
N−Tm−N(intra)		torsion angles	
N12−Tm−22	78.27(19)	Tm−N12 N11−B	2.0(8)
N12−Tm−32	76.87(18)	Tm−N22 N21−B	1.6(8)
N22−Tm−32	78.19(19)	Tm−N32 N31−B	0.6(9)
$N-Tm-N(inter)_{cis}$		$N-Tm-N(inter)_{trans}$	
N12−Tm−N22′	101.73(19)	N12−Tm−N12′	180.0
N12−Tm−N32′	103.16(18)	N22−Tm−N22′	180.00(18)
N22−Tm−N32′	101.81(19)	N32−Tm−N32′	180.0

the almost identically sized Yb(II) complex $Yb(Tp^{Me2})_2$. The average Ln−N distances are Tm−N, 2.477(6) Å, and Yb−N, 2.483(4) Å, respectively. The difference of 0.14 Å in the Ln−N distances between $Sm(Tp^{Me2,4Et})_2$ (Sm−N, 2.615 Å) and $Tm(Tp^{Me2,4Et})_2$ is exactly what is expected on the basis of the difference between the respective ionic radii.[40] The similarity extends to the intra- and interligand N−Ln−N angles between the above complexes; in particular the small Tm−N−N−B torsional angles (average 1.4(9)°, range 0.6−2.0°) mirror those seen in $Sm(Tp^{Me2,4Et})_2$ (average 5.6(18)°, range 2.2−8.0°). Also, just as in the latter complex, the ethyl groups are rotated approximately perpendicular to the linear B−Tm−B axis, with two oriented toward each other and one away.

Computational Studies on $Tm(Tp^{Me2})_2$, $Tm(Tp^{Me2,4Et})_2$, and $Ln(Tp^{iPr2})_2$ (Ln = Sm, Tm). Taking into account the above experimental data, DFT calculations were carried out in order to establish the origin of the unexpected change from the symmetrical sandwich structure of $Ln(Tp^{Me2})_2$ (Ln = Sm, Yb) and $Ln(Tp^{Me2,4Et})_2$ (Ln = Sm, Tm) to the unusual bent geometry of $Ln(Tp^{iPr2})_2$ (Ln = Sm, Tm). In order to establish the suitability of the chosen computational method for the subsequent study of the various structural models of the $Ln(Tp^{iPr2})_2$ compounds, we first compared the optimized computed structures of $Ln(Tp^{Me2})_2$, $Ln(Tp^{Me2,4Et})_2$, **3Sm**, and **3Tm** with those determined by X-ray crystallography.

The calculated structures of $Ln(Tp^{Me2})_2$, $Ln(Tp^{Me2,4Et})_2$, and $Ln(Tp^{iPr2})_2$ (Ln = Tm) are shown in Figures SI 3 and SI 4, respectively, and the key metrical parameters are summarized in Tables SI 3 and SI 4. There is good agreement between the experimental and DFT-optimized structures; the calculated distances are on average 0.08 Å longer and the bond angles between 2° and 4° larger than in the X-ray crystal structures. These differences are consistent with the use of large-core relativistic effective core potentials and the lack of core−valence correlation effects.[43] This agreement with experiment gives us confidence that our computational methods are appropriate for the study of these electronically complex molecular systems.

To understand the peculiar bent geometry observed with the Tp^{iPr2} ligands, we optimized three additional structures: (a) a linear sandwich structure, analogous to that obtained with the Tp^{Me2} ligand, (b) an unsymmetrical structure, similar to that obtained with the $Tp^{tBu,Me}$ ligand, with one normal Tp ligand and the other N-bidentate with a single B−H···Ln agostic interaction, and (c) a $(N_2H)_2$-Tp^{iPr2} structure with two identical Tp^{iPr2} ligands coordinated to the metal center via two nitrogen donor atoms and an agostic B−H interaction. The optimized structures are shown in Figures SI 5 and SI 6, respectively.

It is noteworthy that for the $Ln(Tp^{iPr2})_2$ compounds the optimized linear sandwich structure has its minimum energy with the 3-iPr substituents having a conformation that orients one isopropyl methyl group toward the metal center; the alternate orientation, with the isopropyl C−H bond pointing toward the metal, would result in prohibitive steric congestion between the methyl groups lying in the equatorial plane. Nevertheless, the linear structure is strongly destabilized with respect to the bent geometry by +51.8 kcal mol^{-1} (Tm) and +42.7 kcal mol^{-1} (Sm).

The two structures involving either one (b) or two (c) agostic B−H interactions are also unstable with respect to the bent structure of $Ln(Tp^{iPr2})_2$ by 7.6 and 20.9 kcal mol^{-1} for Sm and by 7.0 and 17.5 kcal mol^{-1} for Tm, respectively. For the $Ln(Tp^{iPr2})_2$ complexes, and unlike for $Ln(Tp^{tBu,Me})_2$, the NBO analysis indicates that the stabilization due to the decrease in steric hindrance around the metal center and the formation of

dx.doi.org/10.1021/ic501816v | Inorg. Chem. 2014, 53, 12066−12075

one agostic B−H bond does not offset the energetic cost of breaking one Ln−N interaction.

In order to identify clearly the origin of the bent structure, two isomeric compounds with less bulky ligands, $Ln(Tp^{Me,iPr})_2$ and $Ln(Tp^{iPr,Me})_2$, were considered. With respect to $Ln(Tp^{iPr2})_2$, in the $Ln(Tp^{Me,iPr})_2$ complex, it is the 3-^{i}Pr groups in the vicinity of the metal center (*proximal*) that are replaced by methyl groups, while for the $Ln(Tp^{iPr,Me})_2$ complex, it is the 5-^{i}Pr groups around the boron atom that are substituted by methyl groups (*distal*). In our calculations, the substitution of the *proximal* 3-^{i}Pr ligands leads to a fully linear structure with a B−Ln−B angle of 180°, both for Sm and Tm (Figure 4a). On the other hand, with substitution of the *distal* 5-^{i}Pr ligands by methyl groups the bent geometry is favored; the B−Ln−B angle does not change, remaining approximately 154° for both metals (Figure 4b).

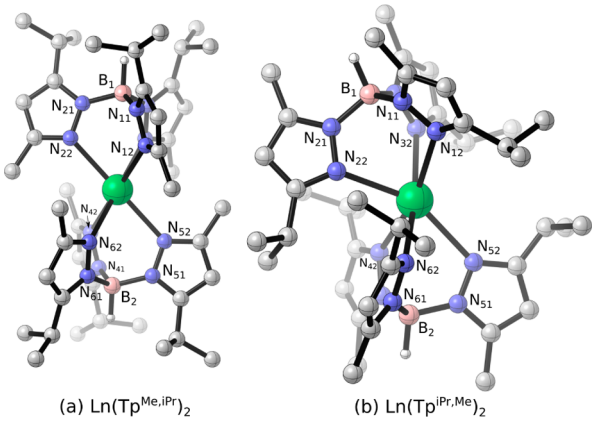

Figure 4. Optimized computed structures (side views) of (a) $Ln(Tp^{Me,iPr})_2$ and (b) $Ln(Tp^{iPr,Me})_2$ compounds. The molecules shown are for Ln = Tm. The Sm complexes adopt similar geometries. In (a) $Ln(Tp^{Me,iPr})_2$, the *proximal* 3-Me groups are close to Ln, and in (b) $Ln(Tp^{iPr,Me})_2$, the *distal* 5-Me groups are close to the B atoms. Hydrogen atoms have been omitted for clarity.

Thus, the origin of the bent structure can be traced to the presence of the *proximal*-3^{i}Pr groups, since decreasing the steric hindrance of the ligands by replacing these substituents by methyl groups leads, in our calculations, to the linear sandwich structure. Although at first sight trivial, the question remains whether the distortion toward the bent structure is purely driven by release of steric hindrance or whether the conformational flexibility of the ^{i}Pr group makes possible additional interactions. We have already seen that the symmetrical linear structure, with the Me groups of the *proximal*-3^{i}Pr pointing toward Ln, is a very high energy structure. However, close examination of the solid-state structures of **3Sm** and **3Tm** and the computed structures reveals that the conformations of the *proximal*-3^{i}Pr groups in the expanded, N12N32N52, and contracted, N22N42N52, faces are different. While those in the expanded face have the 3-^{i}Pr C−H bond pointing toward the metal, those on the contracted face have the C−H pointing toward a nitrogen atom from another Tp^{iPr2} ligand, with which they are in close contact, Figure 5. The relevant atoms and distances (in parentheses are the X-ray values) in complex **3Tm** are N22^{i}PrC−H···N62 2.68 (2.61) Å, N42^{i}PrC−H···N32 2.81 (2.62) Å, and N62^{i}PrC−H···N12 2.89 (2.68) Å. The same is seen in the computed structures of $Ln(Tp^{iPr,Me})_2$ (Figure 4b) with C−H···N distances in the same range, N22^{i}PrC−H···N62 2.64 Å, N42^{i}PrC−H···N32 2.75 Å, and N62^{i}PrC−H···N12 2.97 Å. These C−H···N contacts are in the range of values normally associated with C−H···N hydrogen bonds.[44] Hence these hydrogen-bonding interactions provide additional stabilization in the bent-sandwich structures of $Ln(Tp^{iPr2})_2$ and $Ln(Tp^{iPr,Me})_2$ over and above the release of steric congestion. This further demonstrates the influence of the *proximal* 3-^{i}Pr substituents in the pyrazole ring. Attempts to corroborate the presence of ^{i}PrC−H···N H-bonding by IR spectroscopy proved inconclusive. Although the IR spectra (Figures SI 1and SI 2) show weak peaks at the lower frequency side of the main C−H stretching region of the Tp^{iPR2} ligand, it is not clear that these belong to the, expectedly red-shifted, C−H···N stretches.

To highlight the crucial influence of the two effects (steric and electronic), two virtual, model complexes were considered. In the first one, the three *proximal* 3-^{i}Pr groups in the expanded N12N32N52 face of $Ln(Tp^{iPr,Me})_2$, not involved in any hydrogen bonds, were replaced by methyl ligands (Figure 6a), while, in the second complex, the three *proximal* 3-^{i}Pr groups in the contracted N22N42N62 face, involved in the formation of the hydrogen bonds, were substituted by methyl groups (Figure 6b). Of course, these model complexes do not represent the optimal distribution of three ^{i}Pr groups on a Tp ligand, but they allow us systematically to investigate the role of both electronic and steric effects on the metal coordination

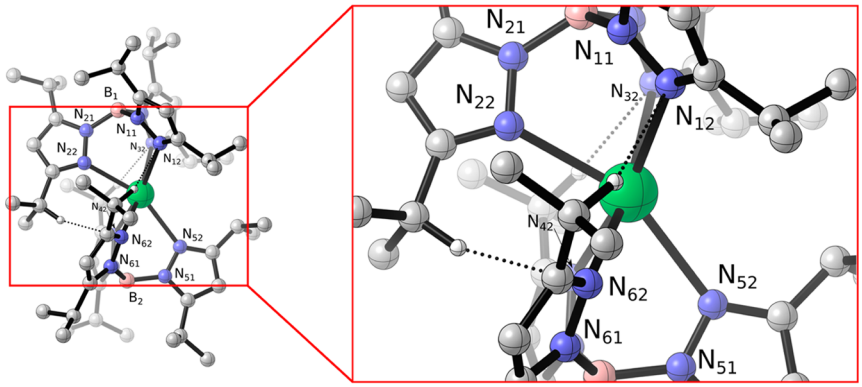

Figure 5. Enlarged side view of the optimized computed structure of $Tm(Tp^{iPr2})_2$ (**3Tm**), showing the close 3-^{i}PrC−H---N contacts on the contracted N22N42N62 face; N22^{i}PrC−H···N62, N42^{i}PrC−H···N32, and N62^{i}PrC−H···N12 (all other H atoms have been omitted for clarity). The $Sm(Tp^{iPr2})_2$ (**3Sm**) compound exhibits similar close contacts.

dx.doi.org/10.1021/ic501816v | *Inorg. Chem.* 2014, 53, 12066−12075

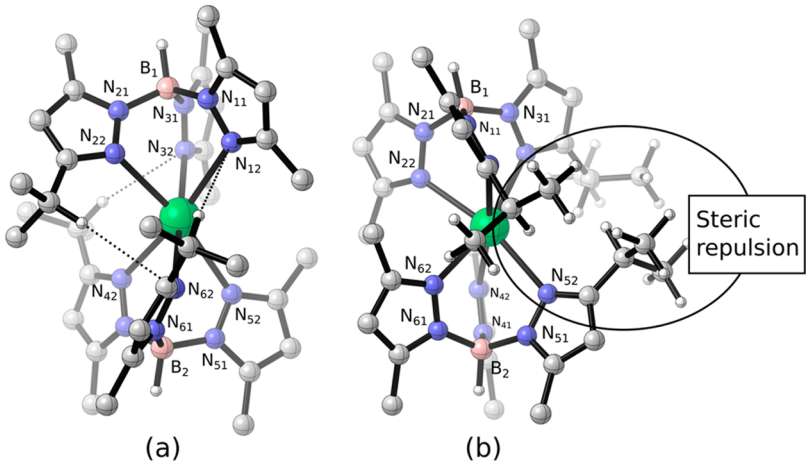

Figure 6. Computed structures (side views) of two model compounds. (a) The 3-^{i}Pr groups on the expanded N12N31N52 face and (b) the 3-^{i}Pr groups on the contracted N22N42N62 face have been replaced by 3-Me substituents, respectively. Also shown are the close 3-^{i}PrC−H---N contacts in the former (N22^{i}PrC−H···N62, N42^{i}PrC−H···N32, and N62^{i}PrC−H···N12) and steric repulsion between the 3-^{i}Pr groups in the later; all other H atoms have been omitted for clarity.

geometry and to probe the origin of the unusual B−Ln−B angle. Remarkably, in both cases, the structures remain bent with a B−Ln−B angle around 162° and 166° respectively for Sm and Tm. The bent geometry of the first structure is associated with the presence of the close C−H···N contacts (Figure 6a)—a nonclassical hydrogen bond—whereas the second is the result of steric repulsion between the *proximal* 3-^{i}Pr substituent on each Tp ligand that are facing each other (Figure 6b). Therefore, the "bent sandwich-like" coordination geometry of Ln(Tp^{iPr2})$_2$ is intrinsically linked to the nature and conformational flexibility of the ^{i}Pr groups, which induce sufficient steric repulsion between the two Tp^{iPr2} ligands to destabilize the symmetrical linear geometry but also allow the formation of 3-^{i}PrC−H···N hydrogen bonds, leading to further stabilization of the bent geometry.

The identification of secondary H-bonding, revealed from the computational work, as a stabilizing influence of the unusual coordination geometry of Ln(Tp^{iPr2})$_2$ (Ln = Sm, Tm) is yet another demonstration of the pervasive presence and importance of H-bonds in just about all aspects of chemistry.[45] Of course other nonbonding interactions are of import also, and properly accounting for these effects remains a challenge for computational methods. There is much current effort directed to remedy this situation.[46,47]

Solid-State Structure of [Tm(Tp^{iPr2})$_2$]I (3Tm^{+}). From some preparations of Tm(Tp^{iPr2})$_2$ (**3Tm**), colorless crystals were also isolated. To establish the nature of the compound, single-crystal X-ray diffraction was carried out, which showed that it was the oxidized complex [Tm(Tp^{iPr2})$_2$]I (**3Tm^{+}**). The solid-state structure consists of well-separated [Tm(Tp^{iPr2})$_2$]$^{+}$ cations and iodide counterions with no short contacts between iodide and the Tm(III) center.

The structure of **3Tm^{+}** is shown in Figure 7, while the metrical parameters are also listed in Table 1. The molecular geometry is again of the "bent-sandwich" type, with a B1−Tm−B2 angle of 152.59(5)°, being close to the value seen in **3Tm**. Though bent, the geometry shows more significant deviation from the approximate C_s symmetry of complexes **3Ln**. Thus, both N52 and N22 deviate more than 0.3 Å from the B1TmB2 plane, Table SI 1, and the deviation is in the opposite direction; the distortion tends toward C_2 symmetry, as seen with Sm(Tp^{Me2})$_2$X complexes.[28] The view in Figure 7, with the B1TmB2 plane perpendicular to the page, illustrates this and can be compared with the similar view of **3Tm** shown in Figure 2b. As with the **3Ln** complexes, the bent geometry results in an expansion of the "front" N12N32N52 and contraction of the "back" N22N42N62 faces, but this also is not as regular as with **3Ln**. This is shown by the respective N−Tm−N(interligand)$_{cis}$ angles: while the angles N12−Tm−N52/N32−Tm−N52 in the expanded and N22−Tm−N42/N22−Tm−N62 in the contracted faces of **3Tm** are very similar, the same pair of angles are some 7° different in **3Tm^{+}**: 111.87(6)/119.03(6)° and 85.61(5)/78.70(5)°, respectively.

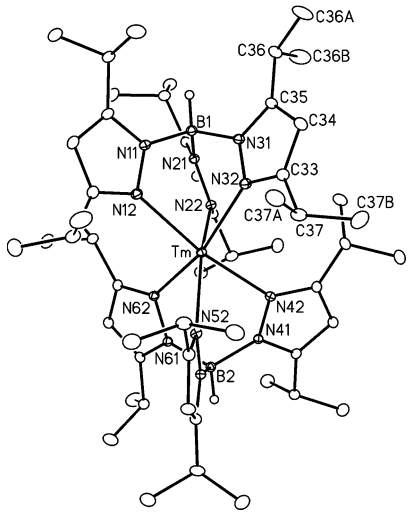

Figure 7. Molecular structure of **3Sm^{+}**, view perpendicular to the N12N32N52 plane (front view), as in Figure 2b. The atoms are drawn with 20% probability ellipsoids. Hydrogen atoms have been omitted for clarity.

A major reason for the differences in bending and the more irregular geometry is undoubtedly the more congested nature of **3Tm^{+}** compared to **3Tm**, due to the smaller size of Tm(III) and the shorter Tm−N distances in the former. Indeed the 0.15 Å decrease in the Tm−N distances from **3Tm** to **3Tm^{+}** corresponds exactly to the expected change in six-coordinate ionic radius between the two ions.[40]

dx.doi.org/10.1021/ic501816v | *Inorg. Chem.* 2014, 53, 12066−12075

The computational study, carried out on the cationic system, again corroborated the bent geometry (see Table SI 4) and also revealed close 3-^{i}PrC−H···N contacts in the contracted N22N42N62 face (X-ray distances in parentheses): N22^{i}PrC−H···N42 2.47 (2.70) Å, N42^{i}PrC−H···N32 2.81 (2.77) Å, and N62^{i}PrC−H···N12 2.47 (2.82) Å. We conclude that in **3Tm**$^{+}$ also the bending can be ascribed to the synergistic effect of steric repulsions between the ^{i}Pr substituents (increased with respect to the neutral system by the shrinkage of the metal coordination sphere in the cationic system) and the presence of hydrogen bonds.

CONCLUSIONS

We have shown that it is possible to prepare bis-scorpionate complexes of the highly reducing thulium(II) ion. Disappointingly, these complexes have proved to be thermally unstable. Nevertheless we have obtained structural, spectroscopic, and computational data that reveal unexpected features, in particular the bent sandwich-like geometry of the Ln(Tp^{iPr2})$_2$ (**3Sm**, **3Tm**) complexes and the occurrence of an unexpected internal C−H···N interaction. The effect of the latter is to lend additional stabilization to this, previously unseen, distortion in the coordination sphere of bis-scorpionate metal complexes. This distortion does *not* arise from metal−ligand bonding, but rather is driven by the interplay of repulsive clashes between bulky substituents *and* the conformational flexibility of the 3-^{i}Pr pyrazolyl substituents that allows for favorable ^{i}PrC-H···N interactions to develop. The conformational flexibility of some 3-R substituents calls into question estimation of steric bulk of scorpionate ligands based simply on accepted cone angle values. Subtle trade-offs between conformations of substituents can render such judgments suspect.

The success of the calculations in reproducing some of the more subtle features of the coordination sphere is a testament to the maturity of DFT calculations in coping with such complex electronic systems. The results presented here are a further illustration of the remarkable flexibility of the pyrazolylborate ligands. It is this flexibility that allows for a far richer variety of coordination geometries for homoleptic bis-scorpionate metal complexes compared to the related MX_2 and $M(C_5R_5)_2$ compounds (X = halide, R = Me, ^{i}Pr, Ph, and 4-nBuPh; M = alkaline earth and Eu, Sm, Yb). Furthermore, it is noteworthy that the combination of steric bulk/secondary H-bonding that, in the case of the planar cyclopentadienyl ligands, resulted in a change from bent- to parallel-sandwich geometry produced the opposite effect with the tripodal Tp^{iPr2} ligand. This vividly demonstrates how the subtle interplay between nonbonding and secondary H-bonding can have a profound effect on the geometry of metal compounds and, indeed, on their structures in general.

EXPERIMENTAL SECTION

General Procedures. All preparations and subsequent manipulations were carried out in a Vacuum Atmospheres glovebox, model HE-553-2, in an atmosphere of helium/argon. THF, diethyl ether, toluene, hexane, and pentane were dried by standard methods and degassed before use. Deuterated solvents, benzene-d_6 and toluene-d_8, were dried over Na or Na/K alloy and distilled before use. Samarium and thulium metals were purchased from HEFA Rare Earth Canada, Co. Ltd., and fresh filings were used for the synthesis of THF solutions of SmI_2[48] and TmI_2.[49] KTp^{Me2,4Et} was prepared as previously described[28] with the following modification: 3-ethylpentane-2,4-dione was prepared by alkylation of pentane-2,4-dione with ethyl iodide using anhydrous sodium carbonate in acetone.[50] Diisopropylpyrazole was purchased from TCI America, and KTp^{iPr2} was prepared by the published procedure of Kitajima,[51] with the following modification: instead of crystallization, excess diisopropylpyrazole was removed by careful, high-vacuum sublimation, resulting in a higher yield of KTp^{iPr2}.

NMR spectra were recorded on Varian Inova 300, 400, or 500 MHz instruments, with shifts reported relative to residual solvent peaks. IR spectra of Ln(Tp^{iPr2})$_2$ (**3Sm**, **3Tm**) were recorded as cast film from pentane, on a Thermo Scientific, Nicolet 8700 FT IR instrument, with KCl plates protected by being sandwiched between O-rings. Elemental microanalyses were performed on a Carlo Erba (Thermo Fisher Scientific) CHNS-O EA1108 elemental analyzer by the staff of the Analytical and Instrumentation Laboratory, University of Alberta.

Synthetic Procedures. *Sm(Tp^{iPr2})$_2$ (**3Sm**).* A THF solution (6 mL) of KTp^{iPr2} (1.009 g, 2.00 mmol) was added dropwise to a freshly prepared THF solution (25 mL) of SmI_2 (1.00 mmol) at room temperature. The initial blue-green color of SmI_2 quickly turned very dark green, accompanied by the formation of a white precipitate of KI. The mixture was stirred for 1 h and centrifuged to remove the KI precipitate. Removal of the THF solvent under vacuum resulted in the formation of a very viscous, dark green oil, which upon further drying produced a dark green, foamy substance; 1.04 g (95% yield of the crude Sm(Tp^{iPr2})$_2$ (**3Sm**)). The crude product was dissolved in 6 mL of pentane, filtered through a plug of glass microfiber filter, and stored in a −35 °C refrigerator for 2 days. The green supernatant was pipetted off, and the dark green precipitate dried under vacuum, yielding only 107 mg of still somewhat sticky, solid **3Sm**. Obtaining better quality solid **3Sm** proved difficult due to the very high solubility of **3Sm** even in hydrocarbon solvents. Eventually, dissolution of the green solid, after removing pentane from the above supernatant, in 2 mL of ether, followed by addition of 1 mL of hexamethyldisiloxane (HMDSO), concentration at room temperature, and a further 2 days in a −35 °C refrigerator, resulted in the precipitation of dark green, solid **3Sm** (470 mg, 43% yield), with satisfactory EA. From one such crystallization, pure crystals of **3Sm** sufficient for X-ray crystallography and NMR characterization were also obtained. Dark green **3Sm** is stable at room temperature for a few hours and at −35 °C for weeks, but shows some decomposition to a white solid of unknown composition.

^{1}H NMR (400 MHz, C_7D_8, 25 °C, δ ppm): −2.11 (br s, 2H, B*H*), −0.85 (d, 36H, 5-^{i}PrC*H*3), −0.08 (s, 6H, 5-^{i}PrC*H*), 3.35 (s, 6H, 4-pzC*H*), 5.41 (d, 36H, 3-^{i}PrC*H*3), 14.15 (s, 6H, 3-^{i}PrC*H*). ^{13}C{^{1}H} NMR (125.7 MHz, C_7D_8, 25C, δ ppm): 19.65 (6C, 5-^{i}PrCH), 26.03 (12C, 5-^{i}PrCH3), 41.54 (12C 3-^{i}PrCH3), 53.57 (6C, 4-pzCH), 70.50 (6C, 3-^{i}PrCH), 144.74 (6C, 5-pzC), 184.12 (6C, 3-pzC). ^{11}B{^{1}H} NMR (128.3 MHz, C_7D_8, −80 °C, δ ppm): −79.6 (br s). IR, ν(B−H): 2553 and 2492 cm^{-1}. Anal. Calcd for $C_{54}H_{92}B_2N_{12}Sm$: C, 59.98; H, 8.58; N, 15.54. Found: C, 59.50; H, 8.44; N, 14.92.

*Tm(Tp^{iPr2})$_2$ (**3Tm**).* Solid KTp^{iPr2} (2.86 g, 5.66 mmol) was added in small portions at room temperature to freshly prepared TmI_2 (2.83 mmol), slurried in 15 mL of THF. The mixture immediately turned from deep green to red-brown and to red. The mixture was stirred for 10−30 min, and the THF removed under vacuum. The sticky product was extracted with 3 × 10 mL of pentane and centrifuged. The plum-red supernatant was concentrated to ca. 5 mL and kept in the −35 °C refrigerator for several days. The precipitated plum-red solid was isolated by pipetting off the supernatant liquid and drying the solid under dynamic vacuum; 1.32 g, 42% yield. The resulting Tm(Tp^{iPr2})$_2$ (**3Tm**) is sufficiently pure for further reactions. Small amounts of crystalline **3Tm** can be obtained from either concentrated pentane or pentane/HMDSO solutions kept at −35 °C. These crystallizations were also accompanied by the formation of a small amount of white solid material of unknown composition, giving evidence of the thermally sensitive nature of **3Tm**. Solid **3Tm** can be kept at −35 °C for at least a week without noticeable change in color; solutions in benzene are stable enough for NMR analysis, but with time and even at −35 °C the compound decomposes to a white solid of unknown composition. Several attempts were made to obtain elemental analysis of **3Tm**, on different samples, but were frustrated by the extreme sensitivity of the compound.

dx.doi.org/10.1021/ic501816v | *Inorg. Chem.* 2014, 53, 12066−12075

^{1}H NMR (500 MHz, C_6D_6, 25 °C, δ ppm): −34.79 (br s, 2H, B*H*), −12.55 (s, 6H, 5-^{i}PrC*H*), −5.08 (s, 36H, 5-^{i}PrC*H3*), 4.75 (s, 6H, 4-pzC*H*), 16.64 (s, 36H, 3-^{i}PrC*H3*), 53.18 (s, 6H, 3-^{i}PrC*H*). ^{11}B{^{1}H} NMR (159.8 MHz, C_6D_6, 25 °C, δ ppm): −102.1 (br s). IR, ν(B−H): 2555 and 2468 cm^{-1} Anal. Calcd for $C_{54}H_{92}B_2N_{12}Sm$: C, 58.96; H, 8.43; N, 15.28.

*Tm(Tp^{Me2,4Et})$_2$ (**4Tm**).* Solid KTp^{Me2,Et} (0.62 g, 1.46 mmol) was added in small portions to a solution of freshly prepared TmI_2 (0.73 mmol) in 40 mL of DME at ca. −40 °C. The dark green solution was allowed to warm slowly to room temperature and stirred for another 0.5 h. During that time, some white solid precipitated. The reaction mixture was filtered, and the filtrate dried under vacuum, to afford **4** as dark green solid (0.60 g, 0.64 mmol, 88% yield). Complex **4** is thermally unstable, even at −35 °C. When stirred in DME at room temperature, a white solid of unknown composition forms, and the same happens with solid **4Tm**, kept at −35 °C when redissolved in DME or THF. Single crystals of **4** suitable of X-ray analysis were grown from a solution of DME and toluene (4:1) at −35 °C. ^{1}H NMR (C_6D_6, 27 °C, δ ppm): 44.55 (br, 18H, 3-*Me*-Tp^{Me2,4Et}), 5.27 (br, 12H, 4−C*H*$_2$CH$_3$-Tp^{Me2,4Et}), 3.82 (br, 18H, 4-CH$_2$C*H*$_3$-Tp^{Me2,4Et}), −14.17 (br, 18H, 5-*Me*-Tp^{Me2,4Et}). Anal. Calcd for $C_{46}H_{78}B_2N_{12}O_2Tm$: C, 54.07; H, 7.69; N, 16.45. Found: C, 53.88; H, 7.49; N, 16.61.

X-ray Crystallographic Studies. Crystals suitable for single-crystal X-ray diffraction studies were obtained as described in the Experimental Section. The crystals were manipulated in the glovebox, coated with Paratone-N oil, and transferred to a cold gas stream on the diffractometer. Data were collected on a Bruker D8/APEX II CCD diffractometer. (Programs for diffractometer operation, data collection, data reduction, and absorption correction were those supplied by Bruker.) The data were corrected for absorption by the Gaussian integration (face-index) method. See Table SI 2 in the Supporting Information for summaries of crystal data.

The structures of compounds **3Sm**, **3Tm**, and **3Tm**$^+$ were solved by a Patterson/structure expansion (DIRDIF-2008),[52] and that of **4Tm** by direct methods.[53] Refinement was completed by full-matrix least-squares on F^2 using the program SHELXL-97.[53] Complex **4** crystallized with one molecule of dimethoxyethane. Attempts to refine peaks of residual electron density as disordered or partial-occupancy solvent dimethoxyethane oxygen or carbon were unsuccessful. The data were corrected for disordered electron density through the use of the SQUEEZE procedure[54] as implemented in PLATON.[55,56] A total solvent-accessible void volume of 542 Å^3 with a total electron count of 110 (consistent with two molecules of solvent dimethoxyethane or one molecule per formula unit of **4**) was found in the unit cell.

■ ASSOCIATED CONTENT

Ⓢ Supporting Information

Simplified diagrams of complexes and ligands discussed in the paper. Tables of plane calculations, X-ray data, and CIF files for complexes **3Sm**, **3Tm**, **3Tm**$^+$, IR spectra of Ln(TpiPr$_2$)$_2$, and **4Tm**. Computational details, tables of computed distances and angles, figures of IR spectra of Ln(Tp^{iPr2})$_2$, and optimized computed structures of Ln(Tp^{Me2})$_2$, Ln(^{TpMe2,4Et})$_2$, Ln(Tp^{iPr2})$_2$ (bent and linear) and the two structures involving formation of one and two B−H···Ln agostic interactions (Ln = Sm, Tm), and energies and cartesian coordinates for all computed structures. This material is available free of charge via the Internet at http://pubs.acs.org.

■ AUTHOR INFORMATION

Corresponding Authors

*E-mail: a.sella@ucl.ac.uk (A.S.).
*E-mail: laurent.maron@irsamc.ups-tlse.fr (L.M.).
*E-mail: joe.takats@ualberta.ca (J.T.).

Present Addresses

‖Aurélien Momin: Lycée Baimbridge, Boulevard des Héros, F-97139 Les Abymes, Guadeloupe.

#Lee Carter: Faculty of Law, University of Calgary, Murray Fraser Hall, 2500 University Drive NW, Calgary, AB T2N 1N4, Canada.

△Stephanie Labouille: School of Chemistry and Centre for Computational Chemistry, University of Bristol, Cantock's Close, Bristol BS8 1TS, United Kingdom.

Author Contributions

The experimental work was carried out by A.M., L.C., and Y.Y. A.M. was cosupervised by J.T. and F.N., and L.C. and Y.Y. by J.T. The calculations and analysis were done by S.L. and I.d.R.; L.M. supervised S.L. and discussed the results with I.d.R. The crystal structures were determined by R.McD. The theoretical part of the manuscript was written by L.M. and I.d.R., and the rest by A.S. and J.T., with contributions from the other authors. We thank the Reviewers for their careful work and perceptive comments.

Notes

The authors declare no competing financial interest.

■ ACKNOWLEDGMENTS

J.T. is grateful to NSERC Canada (Discovery Grant) and the University of Alberta for financial support. L.M. is a member of the Institute Universitaire de France and also acknowledges the Humboldt Fundation for a grant for experienced researchers.

■ REFERENCES

(1) Gillespie, R. J.; Hargittai, I. *The VSEPR Model of Molecular Geometry*; Allyn & Bacon: Boston, 1991.
(2) Wharton, L.; Berg, R. A.; Klemperer, W. *J. Chem. Phys.* **1963**, *39*, 2023.
(3) Hargittai, M. *Chem. Rev.* **2000**, *100*, 2233.
(4) Donald, K. J.; Hoffmann, R. *J. Am. Chem. Soc.* **2006**, *128*, 11236.
(5) Evans, W. J.; Bloom, I.; Hunter, W. E.; Atwood, J. L. *J. Am. Chem. Soc.* **1981**, *103*, 6508.
(6) Evans, W. J.; Hughes, L. A.; Hanusa, T. P. *J. Am. Chem. Soc.* **1984**, *106*, 4270.
(7) Evans, W. J.; Hughes, L. A.; Hanusa, T. P. *Organometallics* **1986**, *5*, 1285.
(8) Andersen, R. A.; Boncella, J. M.; Burns, C. J.; Blom, R.; Haaland, A.; Volden, H. V. *J. Organomet. Chem.* **1986**, *312*, C49.
(9) Andersen, R. A.; Blom, R.; Burns, C. J.; Volden, H. V. *J. Chem. Soc., Chem. Commun.* **1987**, 768.
(10) Williams, R. A.; Hanusa, T. P.; Huffmann, J. C. *Organometallics* **1990**, *9*, 1128.
(11) Kaltsoyannis, N.; Russo, M. R. *J. Nucl. Sci. Technol.* **2002**, 393.
(12) Bytheway, I.; Popelier, P. L. A.; Gillespie, R. J. *Can. J. Chem.* **1996**, *74*, 1059.
(13) Timofeeva, T. V.; Lii, J. H.; Allinger, N. L. *J. Am. Chem. Soc.* **1995**, *117*, 7452.
(14) Hollis, T. K.; Burdett, J. K.; Bosnich, B. *Organometallics* **1993**, *12*, 3385.
(15) Kaupp, M.; Schleyer, P. R.; Dolg, M.; Stoll, H. *J. Am. Chem. Soc.* **1992**, *114*, 8202.
(16) Labouille, S.; Clavaguéra, C.; Nief, F. *Organometallics* **2013**, *32*, 1265.
(17) Sitzmann, H.; Dezember, T.; Schmitt, O.; Weber, F.; Wolmershäuser, G. *Z. Anorg. Allg. Chem.* **2000**, *626*, 2241.
(18) Sitzmann, H.; Dezember, T.; Ruck, M. *Angew. Chem., Int. Ed.* **1998**, *37*, 3114.
(19) Deacon, G. B.; Forsyth, C. M.; Jaroschik, F.; Junk, P. C.; Kay, D. L.; Maschmeyer, T.; Masters, A. F.; Wang, J.; Field, L. D. *Organometallics* **2008**, *27*, 4772.
(20) Ruspic, C.; Moss, J. R.; Schurmann, M.; Harder, S. *Angew. Chem., Int. Ed.* **2008**, *47*, 2121.
(21) Orzechowski, L.; Piesik, D. F. J.; Ruspic, C.; Harder, S. *Dalton Trans.* **2008**, 4742.

(22) Harder, S.; Naglav, D.; Ruspic, C.; Wickleder, C.; Adlung, M.; Hermes, W.; Eul, M.; Pöttgen, R.; Rego, D. B.; Poineau, F.; Czerwinski, K. R.; Herber, R. H.; Nowik, I. *Chem.—Eur. J.* **2013**, *19*, 12272.
(23) Harder, S.; Naglav, D.; Schwerdtfeger, P.; Nowik, I.; Herber, R. H. *Inorg. Chem.* **2014**, *53*, 2188.
(24) Trofimenko, S. *The Coordination Chemistry of Scorpionates-Polypyrazolylborate Ligands*; Imperial College Press: London, 1999.
(25) Pettinari, C. *Scorpionates II: Chelating Borate Ligands*; Imperial College Press: London, 2008.
(26) Takats, J.; Zhang, X. W.; Day, V. W.; Eberspacher, T. A. *Organometallics* **1993**, *12*, 4286.
(27) Maunder, G. H.; Sella, A.; Tocher, D. A. *J. Chem. Soc., Chem. Commun.* **1994**, 885.
(28) Hillier, A. C.; Zhang; Maunder, G. H.; Liu, S. Y.; Eberspacher, T. A.; Metz, M. V.; McDonald, R.; Domingos, Â.; Marques, N.; Day, V. W.; Sella, A.; Takats, J. *Inorg. Chem.* **2001**, *40*, 5106.
(29) Marques, N.; Sella, A.; Takats, J. *Chem. Rev.* **2002**, *102*, 2137.
(30) Davies, C. E.; Gardiner, I. M.; Green, J. C.; Green, M. L. H.; Hazel, N. J.; Grebenik, P. D.; Mtetwa, V. S. B.; Prout, K. *J. Chem. Soc., Dalton Trans.* **1985**, 669.
(31) Domingos, Â.; Lopes, I.; Waerenborgh, J. C.; Marques, N.; Lin, G. Y.; Zhang, X. W.; Takats, J.; McDonald, R.; Hillier, A. C.; Sella, A.; Elsegood, M. R. J.; Day, V. W. *Inorg. Chem.* **2007**, *46*, 9415.
(32) Zhang, X. W.; Takats, J.; McDonald, R. *New J. Chem.* **1995**, *19*, 573.
(33) Fujisawa, K.; Ono, T.; Ishikawa, Y.; Amir, N.; Miyashita, Y.; Okamoto, K.-I.; Lehnert, N. *Inorg. Chem.* **2006**, *45*, 1698.
(34) Cheng, J.; Ferguson, M. J.; Takats, J. *J. Am. Chem. Soc.* **2010**, *132*, 2.
(35) Reinaud, O. M.; Theopold, K. H. *J. Am. Chem. Soc.* **1994**, *116*, 6979.
(36) Bleaney, B. R. *J. Magn. Reson.* **1972**, *8*, 91.
(37) Piguet, C.; Geraldes, C. F. G. C. In *Handbook of Chemistry and Physics of the Rare Earths*; Gschneider, K., Jr.; Bunzli, J.-C.; Pecharsky, V. K., Eds.; Elsevier BV: North-Holland, 2003; Vol. *33*, pp 353−463.
(38) Reger, D. L.; Huff, M. F.; Rheingold, A. L.; Haggerty, B. S. *J. Am. Chem. Soc.* **1992**, *114*, 579.
(39) Cowley, A. H.; Geerts, R. L.; Nunn, C. M.; Carrano, C. J. *J. Organomet. Chem.* **1988**, *341*, C27.
(40) Shannon, R. D. *Acta Crystallogr.* **1976**, *A32*, 751.
(41) Cheng, J.; Takats, J.; Ferguson, M. J.; McDonald, R. *J. Am. Chem. Soc.* **2008**, *130*, 1544.
(42) Nief, F. In *Handbook on the Physics and Chemistry of Rare Earths*; Gschneider, K., Jr.; Bunzli, J.-C.; Pecharsky, V. K., Eds.; Handbook on the Physics and Chemistry of Rare Earths; Elsevier BV: North-Holland, 2010; Vol. *40*, pp 241−300.
(43) Maron, L.; Eisenstein, O. *J. Phys. Chem. A* **2000**, *104*, 7140.
(44) Taylor, R.; Kennard, O. *J. Am. Chem. Soc.* **1982**, *104*, 5063.
(45) Arunan, E.; Desiraju, G. R.; Klein, R. A.; Sadlej, J.; Scheiner, S.; Alkorta, I.; Clary, D. C.; Crabtree, R. H.; Dannenberg, J. J.; Hobza, P.; Kjaergaard, H. G.; Legon, A. C.; Mennucci, B.; Nesbitt, D. J. *Pure Appl. Chem.* **2011**, *83*, 1619.
(46) Zhao, Y.; Truhlar, D. G. *Acc. Chem. Res.* **2008**, *41*, 157.
(47) Corminboeuf, C. *Acc. Chem. Res.* **2014**, 140321125824001.
(48) Namy, J. L.; Kagan, H. B.; Caro, P. E. *New J. Chem.* **1981**, *5*, 479.
(49) Bochkarev, M. N.; Fagin, A. A. *Chem.—Eur. J.* **1999**, *5*, 2990.
(50) Johnson, A. W.; Markham, E.; Price, R. *Organic Syntheses*; 1973; Collect. Vol. *V*, p 785
(51) Kitajima, N.; Fujisawa, K.; Fujimoto, C.; Morooka, Y.; Hashimoto, S.; Kitagawa, T.; Toriumi, K.; Tatsumi, K.; Nakamura, A. *J. Am. Chem. Soc.* **1992**, *114*, 1277.
(52) Beurskens, P. T.; Beurskens, G.; de Gelder, R.; Smits, J. M. M.; Garcia-Granda, S.; Gould, R. O. The *DIRDIF-2008 program system* Crystallography Laboratory, University of Nijmegen: The Netherlands, 2008. http://www.xtal.science.ru.nl/dirdif/software/dirdif.html.
(53) Sheldrick, G. M. *Acta Crystallogr.* **2008**, *A64*, 112.
(54) van der Sluis, P.; Spek, A. L. *Acta Crystallogr.* **1990**, *A46*, 194.
(55) Spek, A. L. *Acta Crystallogr.* **1990**, *A46*, C36.
(56) Spek, A. L. *J. Appl. Crystallogr.* **2003**, *36*, 7−13.